Draft version February 5, 2008
Preprint typeset using LaTeX style emulateapj v. 6/22/04



# PROBING THE PULSAR WIND NEBULA OF PSR B0355+54

K.E. McGowan[1,2], W.T. Vestrand[3], J.A. Kennea[4], S. Zane[2], M. Cropper[2], F.A. Córdova[5]

*Draft version February 5, 2008*

## ABSTRACT

We present *XMM-Newton* and *Chandra* X-ray observations of the middle-aged radio pulsar PSR B0355+54. Our X-ray observations reveal emission not only from the pulsar itself, but also from a compact diffuse component extending $\sim 50''$ in the opposite direction to the pulsar's proper motion. There is also evidence for the presence of fainter diffuse emission extending $\sim 5'$ from the point source. The compact diffuse feature is well-fitted with a power-law, the index of which is consistent with the values found for other pulsar wind nebulae. The morphology of the diffuse component is similar to the ram-pressure confined pulsar wind nebulae detected for other sources. The X-ray emission from the pulsar itself is described well by a thermal plus power-law fit, with the thermal emission most likely originating in a hot polar cap.

*Subject headings:* pulsars: individual (PSR B0355+54) – stars: neutron – X-rays: stars

## 1. INTRODUCTION

Isolated pulsars constitute one of the most powerful laboratories for studying particle acceleration in astrophysics. A significant fraction of the energy from rotation-powered pulsars is converted into a wind (Rees & Gunn 1974), which travels at a velocity close to the speed of light. The interaction of this pulsar wind with the ambient medium produces a shock and acceleration of the relativistic particles at the shock generates synchrotron emission. This non-thermal diffuse emission manifests itself as a pulsar wind nebulae (PWN) or *plerion* at radio and X-ray energies (e.g. Rees & Gunn 1974; Gaensler 2001). Due to the short synchrotron lifetimes of high energy electrons, X-ray emission from a PWN directly traces the current energetics of the pulsar. The spectral and morphological characteristics of an X-ray PWN therefore reveal the structure and composition of the pulsar wind and the orientation of the pulsar's spin axis and/or velocity vector.

The middle-aged 156 ms radio pulsar PSR B0355+54 is known to emit X-rays (Helfand 1983; Seward & Wang 1988; Slane 1994) and gamma-rays (Bhat et al. 1990). Helfand (1983) reported the first detection in X-rays of the source using data from *Einstein*, stating that emission extended $5'$ from the pulsar. However, Seward & Wang (1988) analyzed the *Einstein* data and concluded that while there was evidence for weak emission $1.7'$ from the source position, emission from the pulsar itself was not detected. Nevertheless, they did not rule out the possibility that the emission could be associated with a PWN. Slane (1994) detected PSR B0355+54 in a 20 ks *ROSAT* observation, but owing to the lack of counts it was not feasible to perform a spectral analysis. The analysis of the *ROSAT* data also led to the detection of faint extended emission $\sim 1.6'$ from the pulsar position, but Slane (1994) did not believe there was enough evidence to support a link between the source and the extended emission.

In this paper, we report on *XMM-Newton* and *Chandra* observations of PSR B0355+54 which we use to investigate the presence of diffuse emission that can be attributed to a PWN.

## 2. OBSERVATIONS AND DATA REDUCTION

PSR B0355+54 was observed with *XMM-Newton* on 2002 February 10 for 29 ks. We used data from the European Photon Imaging Camera (EPIC) PN instrument (Strüder et al. 2001) for the spatial, spectral and timing analysis. The PN was configured in *small window* mode and the thin blocking filter was used. Data from the MOS1 instrument (Turner et al. 2001) was also used for the spatial analysis. The MOS1 was operated in *full window* mode with the medium filter. We reduced the EPIC data with the *XMM-Newton* Science Analysis System (SAS version 6.1.0). In order to maximize the signal-to-noise ratio for our *XMM-Newton* observation, we filtered the data to include only single, double, triple and quadruple photon events for the MOS1, and only single and double photon events for the PN. Data were filtered to exclude events that may be incorrect, for example those next to the edges of the CCDs and next to bad pixels. We only included photons with energies in the range $0.3 - 10$ keV.

PSR B0355+54 was observed for 66 ks on 2004 July 16 with the ACIS-S array on *Chandra* in the very faint timed exposure imaging mode. We performed standard data processing using CIAO version 3.2. The data were filtered to restrict the energy range to $0.3 - 10$ keV and to exclude times of high background.

## 3. SPATIAL ANALYSIS

Initial inspection of the images created from the EPIC-PN and EPIC-MOS1 data show relatively strong emission at the pulsar position and evidence for extended emission near to PSR B0355+54 (see Figure 1, top panel). We generated a mosaic of the PN and MOS1 im-

[1] School of Physics and Astronomy, Southampton University, Southampton, UK
[2] Mullard Space Science Laboratory, University College of London, UK
[3] Los Alamos National Laboratory, Los Alamos, NM 87545
[4] Pennsylvania State University, 525 Davey Laboratory, University Park, PA 16802, USA
[5] Chancellor's Office, University of California, Riverside, CA 92521
Electronic address: kem@astro.soton.ac.uk

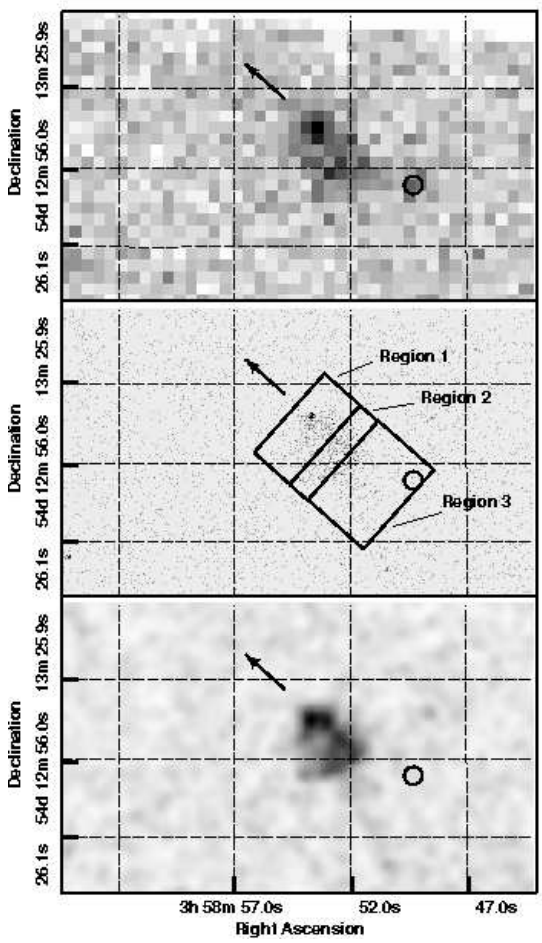


FIG. 1.— X-ray detection of PSR B0355+54 and its diffuse emission. Top panel: Gray-scale plot of the $0.3-10$ keV *XMM-Newton* PN image. Middle panel: Gray-scale plot of the $0.3-10$ keV *Chandra* ACIS image. The boxes define the regions used to extract spectra for the diffuse emission. Bottom panel: The same image as the middle panel with the contribution from the X-ray point source removed. The image is smoothed with a Gaussian of width $\sim 2''$. The arrow shows the direction of the proper motion of the pulsar and has a length of $20''$. The circle marks the "south west" source (see Section 3).

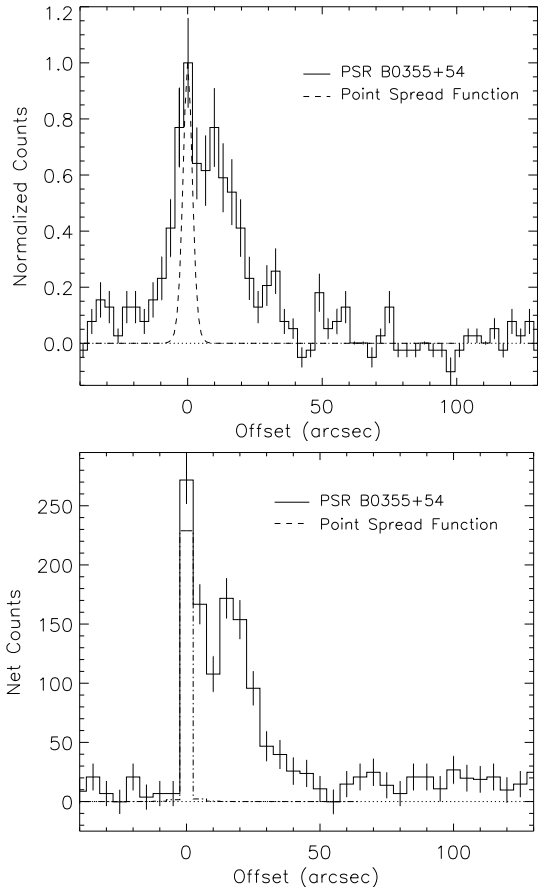


FIG. 2.— X-ray emission from PSR B0355+54 as a function of distance from the point source along the direction of the proper motion of the pulsar (solid line), compared to the instrument PSF determined at 1.5 keV and the location of the pulsar (dashed line). Top panel: *XMM-Newton* PN. Bottom panel: *Chandra* ACIS.

ages and measured the X-ray source positions using the SAS source detection tool EDETECT_CHAIN. We compared the positions of the field stars in our observation with the positions from optical catalogs to determine an astrometric correction. This correction was applied to the X-ray coordinates of the pulsar, resulting in R. A. $= 03^{\rm h}58^{\rm m}53\overset{\rm s}{.}73$, decl. $= +54°13'12\overset{''}{.}12$ (J2000), with an rms error of $0\overset{''}{.}78$. This position lies $1\overset{''}{.}6$ from the radio position.

To confirm the presence and examine the extent of the diffuse emission in the *XMM-Newton* data we have compared the detected PN emission with that for a point source. We calculated the intensity for the pulsar by using bilinear interpolation at regularly spaced points along the direction of proper motion of PSR B0355+54 (Chatterjee et al. 2004). We compared this profile with the *XMM-Newton* point-spread function (PSF) for the PN at 1.5 keV, which we generated using the King profile parameters included in the *XMM-Newton* calibration file "XRT3_XPSF_0006.CCF.plt"[6]. In Figure 2 (top panel) we show the profiles for the pulsar and the PN PSF.

The positions of the X-ray sources for the ACIS data were determined using the CIAO source detection tool WAVDETECT. The image does not contain enough sources with known counterparts to perform an astrometric correction to the coordinates. A point source is detected at R. A. $= 03^{\rm h}58^{\rm m}53\overset{\rm s}{.}70$, decl. $= +54°13'13\overset{''}{.}87$ (J2000), which is $0\overset{''}{.}14$ away from the radio pulsar position. This source is consistent with being the X-ray counterpart of the pulsar.

The ACIS image also reveals a faint tail of emission in the opposite direction to the pulsar's proper motion (see Figure 1, middle and bottom panels). Again we determined the net counts from the source and diffuse emission at regularly spaced intervals along the direction of the pulsar's proper motion. We generated a PSF for PSR B0355+54 using the *Chandra* PSF library evaluated at 1.5 keV and the location relevant to our source. The PSF was normalized to the total counts in PSR B0355+54. We calculated the net counts for the PSF in the same intervals as for PSR B0355+54. The source and PSF profiles are shown in Figure 2 (bottom

[6] See http://xmm.vilspa.esa.es/docs/documents/CAL-SRN-0100-0-0.ps.gz for more information

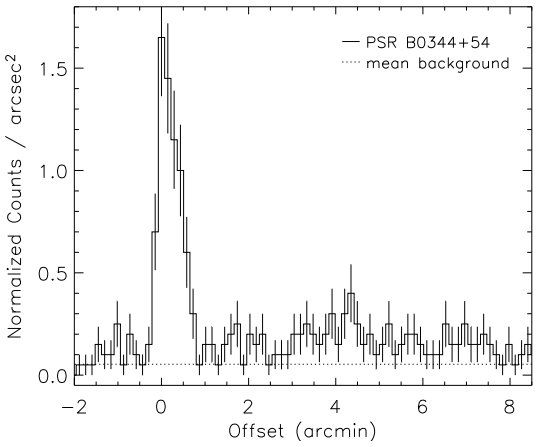


FIG. 3.— *XMM-Newton* MOS1 X-ray emission from PSR B0355+54 as a function of distance from the point source, orientated 20° further North from the direction of the pulsar's proper motion (solid line), compared to the mean background (dotted line).

panel).

The *XMM-Newton* PN image shows emission $\sim 45''$ south west of the pulsar which could be a source, however, there is no corresponding emission at this position in the *Chandra* ACIS image (see Figure 1). We performed wavelet analysis on the *Chandra* data which confirms there is no source detected. Comparison of the *XMM-Newton* field of PSR B0355+54 with the Digitized Sky Survey does not show any optical source at the position of the south west emission. If the emission in the *XMM-Newton* data is real, it suggests that the diffuse emission could be varying over time.

We smoothed the *Chandra* ACIS image with a Gaussian of width $\sim 2''$ (Figure 1, bottom panel), the resulting image suggests that there are two regions of enhanced diffuse emission – one near to the pulsar and the other $\sim 10''$ away. The intensity profiles for the *XMM-Newton* and *Chandra* data indicate that the core of the X-ray emission lies within $5''$ of the pulsar position. Both emission profiles indicate that the diffuse emission extends out to $\sim 50''$, with the bulk of the emission lying within $20 - 30''$ of PSR B0355+54. The profiles also show evidence for a dip in the emission at $\sim 10''$ agreeing with the smoothed ACIS image.

Detection of emission from PSR B0355+54 at distances of $1.'6$ to $5'$ from the source position i.e. on a larger scale than shown in Figure 1, have been reported by Helfand (1983), Seward & Wang (1988) and Slane (1994), see also Tepedelenlioğlu & Ögelman (2005). Visual inspection of a smoothed version of the MOS1 image indicates that there is a region of enhanced emission extending a few arcminutes south of the pulsar, orientated $\sim 20°$ closer to North than the diffuse emission we have reported above. The intensity of the MOS1 emission in this direction was determined using bilinear interpolation at regularly spaced intervals from the source. We show in Figure 3 the distribution of counts as a function of distance from the source compared to the mean background. Our analysis suggests that there is an excess of counts at $1'$ and $\sim 3 - 5'$ from the point source.

## 4. SPECTRAL ANALYSIS

In order to investigate the properties of the X-ray emission from PSR B0355+54 and the compact ($\leq 50''$) diffuse nebula, we compared the spectra extracted from different spatial regions. Our results from the spatial analysis suggest that the core of the pulsar emission lies within $5''$ of the pulsar's position. However, in the case of the *XMM-Newton* data, this size of aperture does not contain enough counts for a meaningful analysis.

The pulsar spectrum has been extracted from the *XMM-Newton* observation using a circular region of radius $30''$, centered on the pulsar's radio position. The background was extracted from a region of similar size offset from the pulsar position. The total counts contained in the source region is 1143 with an estimated 562 from background. The spectrum was regrouped by requiring at least 50 counts per spectral bin. We created a photon redistribution matrix (RMF) and ancillary region file (ARF) for the spectrum. The subsequent spectral fitting and analysis was performed using XSPEC, version 11.3.1.

We modeled the spectrum in the $0.5 - 9.0$ keV range. Initially we fitted the spectrum with single-component models including absorbed power-law, blackbody and magnetized, pure H atmospheric (Pavlov et al. 1995) models. The spectrum is best-fitted with a power-law with index $\Gamma = 1.5^{+0.5}_{-0.3}$ and column density $N_H = (0.50^{+0.36}_{-0.20}) \times 10^{22}$ cm$^{-2}$. This value for the power-law index is similar to the values found for other PWNe (e.g. Kaspi et al. 2005). The Galactic hydrogen column in the direction of PSR B0355+54 is $N_H = 0.88 \times 10^{22}$ cm$^{-2}$. The fit results in an unabsorbed 0.3–10 keV energy flux of $(2.3^{+1.0}_{-0.7}) \times 10^{-13}$ ergs cm$^{-2}$ s$^{-1}$. We also fitted the spectrum with blackbody plus power-law and atmospheric plus power-law models, both modified by photoelectric absorption. The multi-component models give similar values for reduced $\chi^2$, however the temperatures implied by the fits are poorly constrained. It is likely that the presence of the pulsar wind nebula, and being unable to separate the pulsar core and diffuse emission, effects our ability to constrain the thermal component in the spectral fits of the *XMM-Newton* data. The results of the *XMM-Newton* spectral fitting are given in Table 1. The *XMM-Newton* spectrum with the best-fitting power-law model is shown in Figure 4.

For the *Chandra* data we extracted a spectrum for the core of the pulsar emission from a circular region of radius $5''$ centered on the radio position. An annulus centered on the pulsar position was used to extract the background, with inner and outer radii of $6''$ and $10''$, respectively. We find a total of 244 counts contained in the source region, with 29 counts attributed to background. We created the RMF and ARF files using standard CIAO tools. Before fitting the spectrum we regrouped the data, requiring a minimum of 15 counts per spectral bin.

We fitted the spectrum in the energy range $0.5 - 7.0$ keV using the same models as for the *XMM-Newton* data. In the first instance we let the neutral hydrogen column density be a free parameter; however this led to unreasonably small values for $N_H$. Subsequently we fixed the column density at the value found from the power-law fit to the *XMM-Newton* spectrum of PSR B0355+54. We find that the *Chandra* spectrum can also be characterized by a power-law. The model has a power-law index

TABLE 1
BEST-FIT PARAMETERS FOR THE *XMM-Newton* SPECTRUM OF PSR B0355+54

| Model | $N_H$ ($10^{22}$ cm$^{-2}$) | $\Gamma$ | $T/T^{\infty}_{eff}$ ($10^6$ K) | $\chi^2_\nu$ (dof) | $F_X$ (erg cm$^{-2}$ s$^{-1}$) |
|---|---|---|---|---|---|
| PL | $0.50^{+0.36}_{-0.20}$ | $1.5^{+0.5}_{-0.3}$ | ... | 0.7 (16) | $(2.3^{+1.0}_{-0.7}) \times 10^{-13}$ |
| BB | $< 0.01$ | ... | $11.26^{+1.74}_{-1.51}$ | 1.0 (16) | $(1.4^{+0.1}_{-1.1}) \times 10^{-13}$ |
| BB + PL | $0.23^{+0.69}_{-0.23}$ | $0.8^{+0.3}_{-0.3}$ | $7.66^{+2313}_{-4.64}$ | 0.7 (14) | $(2.0^{+1.0}_{-1.1}) \times 10^{-13}$ |
| NSA | $0.13^{+0.23}_{-0.11}$ | ... | $7.66^{+0.01}_{-2.83}$ | 0.9 (16) | $(1.4^{+0.1}_{-1.3}) \times 10^{-13}$ |
| NSA + PL | $0.49^{+0.21}_{-0.21}$ | $1.5^{+1.0}_{-0.3}$ | $0.64^{+6.83}_{-0.75}$ | 0.8 (14) | $(2.4^{+1.1}_{-1.0}) \times 10^{-13}$ |

NOTE. — The last column is the unabsorbed flux in the 0.3–10 keV range. In the case of the NSA model the mass and radius of the neutron star are fixed at $M_{NS} = 1.4 M_\odot$ and $R_{NS} = 10$ km, respectively, and the magnetic field of the neutron star is fixed at $B = 10^{12}$ G. The errors quoted are the 90% uncertainties.

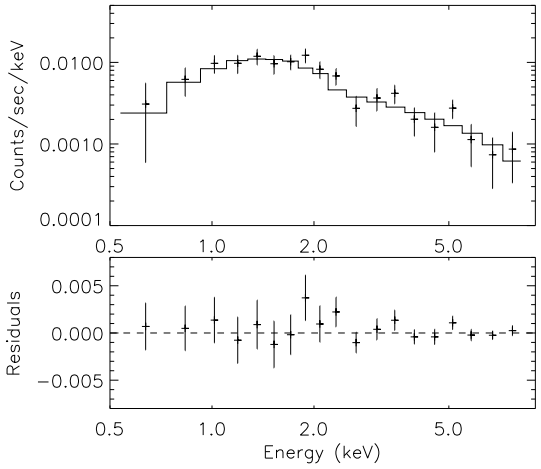


FIG. 4.— The *XMM-Newton* spectrum of PSR B0355+54 with best-fit power-law model. Also shown are the residuals from comparison of the data to the model.

of $\Gamma = 1.9^{+0.4}_{-0.3}$ which is consistent within the 90% uncertainties to the value found from the *XMM-Newton* data. However, in the case of the *Chandra* data we find that a thermal plus power-law model provides a better fit statistically. The data are equally well-fitted by a blackbody plus power-law and a magnetized, pure H atmospheric (Pavlov et al. 1995, "nsa" model in XSPEC) plus power-law model. The results of the *Chandra* spectral fitting are given in Table 2.

For the blackbody plus power-law model the best-fit parameters are a power-law index of $\Gamma = 1.0^{+0.2}_{-1.0}$ and temperature of $T = (2.32^{+1.16}_{-0.81}) \times 10^6$ K. Using a distance to the source of $D = 1.04^{+0.21}_{-0.16}$ kpc (Chatterjee et al. 2004), this implies a blackbody emitting radius of $0.12^{+0.16}_{-0.07}$ km. This value is too small to be reconciled with the radius of the neutron star and would indicate that the origin of the emission is a hot polar cap. We find an unabsorbed 0.3–10 keV energy flux of $(6.4^{+19.3}_{-1.1}) \times 10^{-14}$ ergs cm$^{-2}$ s$^{-1}$. The magnetized, pure H atmospheric plus power-law model best-fit parameters are a power-law index of $\Gamma = 1.5^{+0.5}_{-0.4}$, temperature of $T^{\infty}_{eff} = (0.45^{+0.20}_{-0.22}) \times 10^6$ K, and a radius for the neutron star of $R_{NS} = 7.2^{+7.2}_{-2.2}$ km. For this fit the distance to the source and the mass of the neutron star were fixed at $D = 1.04$ kpc and $M_{NS} = 1.4 M_\odot$, respectively. The magnetic field of the neutron star was fixed at $B = 10^{12}$ G (this is a good approximation since the pulsar magnetic field as inferred from radio timing properties is $B = 8.4 \times 10^{11}$ G, Hobbs et al. 2004; Manchester et al. 2005). The unabsorbed 0.3–10 keV energy flux for this fit is $(1.5^{+54.0}_{-0.7}) \times 10^{-13}$ ergs cm$^{-2}$ s$^{-1}$. The *Chandra* spectrum of the core emission from PSR B0355+54 is shown in Figure 5 with the best-fitting blackbody plus power-law model (top) and magnetized, pure H atmospheric plus power-law model (bottom).

To analyze the compact diffuse emission we created a new events file in which the emission from the pulsar core was removed. We extracted a spectrum for the diffuse component from a rectangular region of $40'' \times 55''$, centered on the emission and orientated along the direction of the pulsar's proper motion. The background was extracted from a region of similar size offset from the diffuse emission. The diffuse component extraction region contains 1207 counts, with an estimated 414 counts due to background. We created the RMF and ARF files using standard CIAO tools. Before fitting the spectrum we regrouped the data, requiring a minimum of 15 counts per spectral bin. We modeled the spectrum over $0.5 - 7.0$ keV with an absorbed power-law, keeping the column density fixed at $N_H = 0.50 \times 10^{22}$ cm$^{-2}$. The best-fit has a power-law index of $\Gamma = 1.4 \pm 0.3$ and unabsorbed 0.3–10 keV energy flux of $(1.7^{+0.8}_{-0.5}) \times 10^{-13}$ ergs cm$^{-2}$ s$^{-1}$.

In order to investigate the possibility of spectral evolution along the extended X-ray emission we created spectra for three regions of the compact diffuse emission. The sizes of the regions were chosen with the aim of having similar numbers of counts in each region. The three extraction regions, orientated along the direction of proper motion, are as follows, region 1: $40'' \times 18''$, contains a total of 396 counts with 130 attributed to background, region 2: $40'' \times 9''$, contains a total of 356 counts with 69 attributed to background, region 3: $40'' \times 28''$, contains a total of 454 counts with 214 attributed to background (see Figure 1 (middle panel)). The background was extracted from the same region as above. We created response files for each region and regrouped the spectra, requiring a minimum of 15 counts per spectral

TABLE 2
Best-fit parameters for the *Chandra* X-ray emission of PSR B0355+54

| Region | Model | $\Gamma$ | $T/T^{\infty}_{eff}$ ($10^6$ K) | $R_{BB}/R_{NS}$ km | $\chi^2_\nu$ (dof) | $F_X$ (erg cm$^{-2}$ s$^{-1}$) |
|---|---|---|---|---|---|---|
| Core | PL | $1.9^{+0.4}_{-0.3}$ | ··· | ··· | 0.5 (34) | $(4.9^{+1.6}_{-0.7}) \times 10^{-14}$ |
| | BB | ··· | $6.73^{+2.32}_{-1.87}$ | $0.01^{+0.03}_{-0.01}$ | 1.4 (34) | $(2.4^{+0.1}_{-0.1}) \times 10^{-14}$ |
| | BB + PL | $1.0^{+0.2}_{-1.0}$ | $2.32^{+1.16}_{-0.81}$ | $0.12^{+0.16}_{-0.07}$ | 0.3 (32) | $(6.4^{+19.3}_{-1.1}) \times 10^{-14}$ |
| | NSA | ··· | 0.48 | 9.5 | 3.6 (34) | $(1.8^{+0.3}_{-0.5}) \times 10^{-13}$ |
| | NSA + PL | $1.5^{+0.5}_{-0.4}$ | $0.45^{+0.20}_{-0.22}$ | $7.2^{+7.2}_{-2.2}$ | 0.4 (32) | $(1.5^{+54.0}_{-0.7}) \times 10^{-13}$ |
| Diffuse – all | PL | $1.4^{+0.3}_{-0.3}$ | ··· | ··· | 1.0 (50) | $(1.7^{+0.8}_{-0.5}) \times 10^{-13}$ |
| Diffuse – 1 | PL | $1.4^{+0.4}_{-0.4}$ | ··· | ··· | 1.0 (16) | $(5.7^{+3.3}_{-1.8}) \times 10^{-14}$ |
| Diffuse – 2 | PL | $1.5^{+0.3}_{-0.3}$ | ··· | ··· | 1.4 (16) | $(7.6^{+3.4}_{-1.9}) \times 10^{-14}$ |
| Diffuse – 3 | PL | $1.2^{+0.5}_{-0.4}$ | ··· | ··· | 1.2 (17) | $(5.3^{+4.4}_{-2.0}) \times 10^{-14}$ |

Note. — The neutral hydrogen column density has been fixed at $N_H = 0.50 \times 10^{22}$ cm$^{-2}$ in all of the fits. The last column is the unabsorbed flux in the 0.3–10 keV range. In the case of the NSA model the distance to the source is fixed at $D = 1.04$ kpc, the mass of the neutron star is fixed at $M_{NS} = 1.4 M_\odot$, and the magnetic field of the neutron star is fixed at $B = 10^{12}$ G. The errors quoted are the 90% uncertainties.

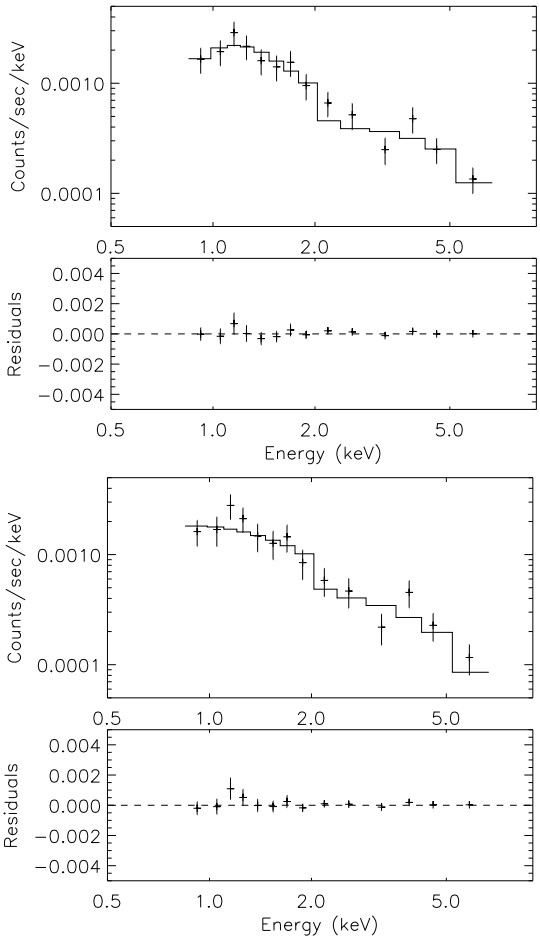


Fig. 5.— The *Chandra* spectrum of the core emission of PSR B0355+54 with best-fit blackbody plus power-law model (top) and magnetized, pure H atmospheric plus power-law model (bottom). Also shown are the residuals from comparison of the data to the model in each case.

bin. The spectra were fitted in the $0.5 - 7.0$ keV energy range with a power-law and fixed column density of $N_H = 0.50 \times 10^{22}$ cm$^{-2}$. We find the best-fit power-law indices for regions 1–3 are $\Gamma = 1.4 \pm 0.4$, $1.5 \pm 0.3$ and $1.2^{+0.5}_{-0.4}$, respectively. Due to the uncertainties on the indices the presence of any spectral variability remains unclear. The unabsorbed 0.3–10 keV energy fluxes are $(5.7^{+3.3}_{-1.8}) \times 10^{-14}$, $(7.6^{+3.4}_{-1.9}) \times 10^{-14}$ and $(5.3^{+4.4}_{-2.0}) \times 10^{-14}$ ergs cm$^{-2}$ s$^{-1}$, respectively. The *Chandra* spectra of the diffuse emission from regions 1–3 are shown in Figure 6 (first–third panel) with the best-fitting power-law models.

We have also tried to determine if there are any spectral changes by using the hardness ratio $h_{2.0}$, which is defined as the ratio of counts above 2.0 keV to that below 2.0 keV. For the whole of the compact diffuse component we find $h_{2.0} = 0.97 \pm 0.09$. Regions 1, 2 and 3 have $h_{2.0} = 1.05 \pm 0.17$, $0.91 \pm 0.13$ and $0.97 \pm 0.18$, respectively. Due to the uncertainties, no particular trends in hardness ratio can be determined from one region to the next.

## 5. TIMING ANALYSIS

We barycentrically corrected the photon arrival times in the *XMM-Newton* PN event file before performing the temporal analysis. We extracted data for the source from circular regions of 15″ and 30″ centered on the pulsar position. The total counts encompassed in these regions are 391 and 1143 respectively, with the background contributing 151 and 562 counts, respectively.

In order to search for an X-ray modulation at the PSR B0355+54 spin frequency, we first determined a predicted pulse frequency at the epoch of our *XMM-Newton* observations, assuming a linear spin-down rate and using the radio measurements (Hobbs et al. 2004; Manchester et al. 2005). We calculate $f = 6.3945388$ Hz at the midpoint of our observation (MJD 52315.7). As glitches and/or deviations from a linear spin-down may alter the period evolution, we then searched for a pulsed signal over a wider frequency range centered on $f = 6.39454$ Hz. We searched for pulsed emission using

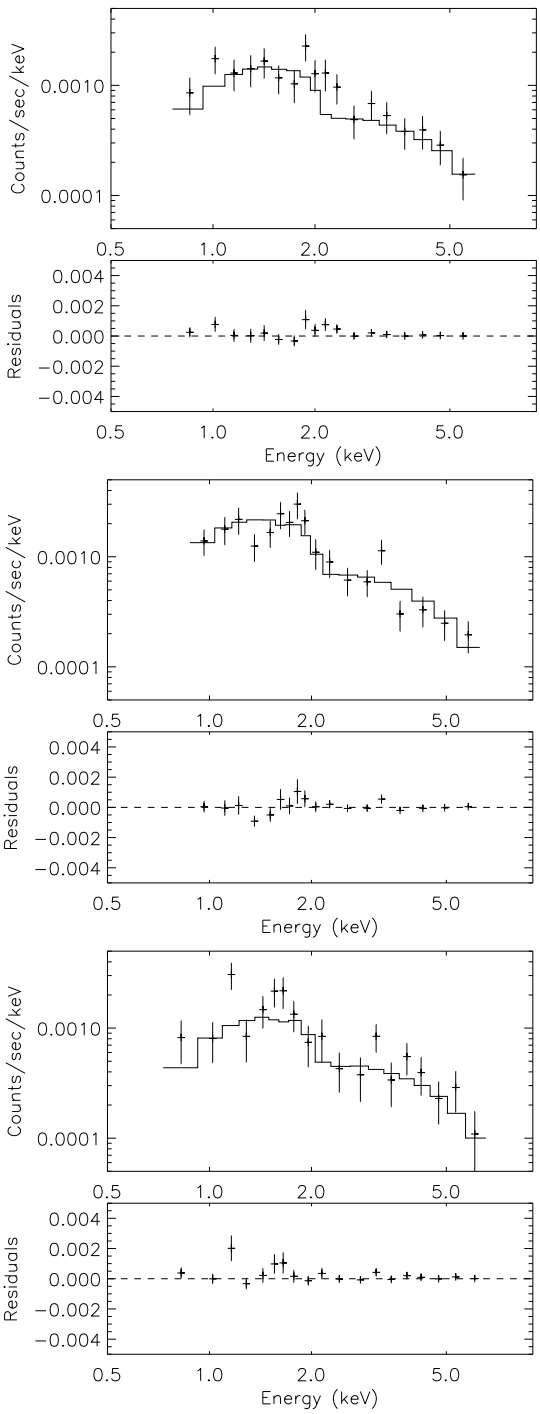


FIG. 6.— Spectral fitting to *Chandra* data of PSR B0355+54. First–third panels: diffuse emission from regions 1–3, respectively, with best fit power-law models. Also shown are the residuals from comparison of the data to the model in each case.

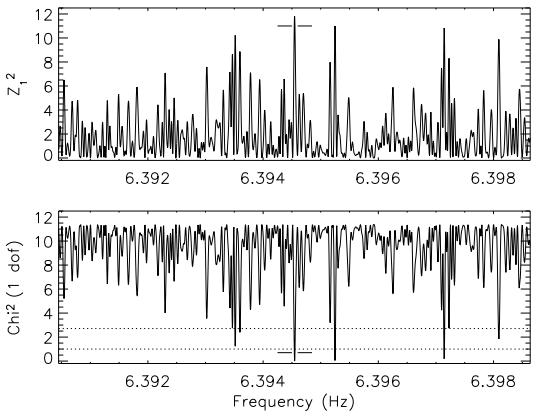


FIG. 7.— $Z_1^2$-test (top) and Maximum Likelihood Periodogram (MLP; bottom) for the PN data of PSR B0355+54. The dominant peak from the $Z_1^2$-test and the corresponding peak in the MLP are marked. The peaks occur at $6.3945447^{+0.0000167}_{-0.0000107}$ Hz and $6.3945467^{+0.00000821}_{-0.00000818}$ Hz, respectively. The dotted lines represent the 68% ($\chi^2 = 2.71$) and 90% ($\chi^2 = 1.0$) confidence levels for the frequencies in the MLP.

two methods. In the first method we implement the $Z_n^2$ test (Buccheri et al. 1983), with the number of harmonics $n$ being varied from 1 to 5. In the second method we calculate the Rayleigh statistic (de Jager 1991; Mardia 1972) and then calculate the maximum likelihood periodogram (MLP; see e.g. Zane et al. 2002) using the $C$ statistic (Cash 1979) to determine significant periodicities in the data sets.

The frequency search of the data extracted from an aperture of radius 30″ does not yield any significant peaks near to the predicted frequency with either search method. From our spatial analysis we know that the core of PSR B0355+54's emission lies within $\sim 5''$ of the pulsar position. We have therefore also searched for pulsed modulations in data extracted from a smaller aperture, however we have used a radius of 15″ as any smaller does not encompass enough counts for a meaningful analysis.

The most significant $Z_n^2$-statistic occurs for $n = 1$. With the number of harmonics equal to one, the $Z_n^2$-statistic corresponds to the well known Rayleigh statistic. We find three peaks with $> 90\%$ significance in the MLP, all with corresponding peaks from the $Z_1^2$-test (see Figure 7). The dominant peak from the $Z_1^2$-test occurs at $6.3945447^{+0.0000167}_{-0.0000107}$ Hz, with the corresponding peak in the MLP occurring at $6.3945467^{+0.00000821}_{-0.00000818}$ Hz. The uncertainties quoted are the 68% confidence limits on the position of the peak. Both frequencies are consistent, within the 68% contour, with the predicted pulse frequency, and with each other within the 90% contour. The second most prominent peak from the $Z_1^2$-test, and the corresponding peak in the MLP, are not consistent with the predicted pulse frequency.

While we have detected a frequency that is in agreement with the predicted pulse frequency for PSR B0355+54 we caution that the $Z_1^2$ peak has a probability of chance occurrence of $3 \times 10^{-3}$. Further observations of the source are needed to show whether the modulation detected is in fact pulsed X-ray emission from PSR B0355+54. We have folded the data on the predicted pulse frequency and the frequency found from the $Z^2$-test (see Figure 8); by fitting the profiles with a sinusoid we find that the modulation amplitude for the former is $25 \pm 7\%$ and $21 \pm 8\%$ for the latter.

## 6. DISCUSSION

Our spatial analysis of the *XMM-Newton* and *Chandra* observations of PSR B0355+54 have not only revealed X-rays from the pulsar, but have provided definitive proof of

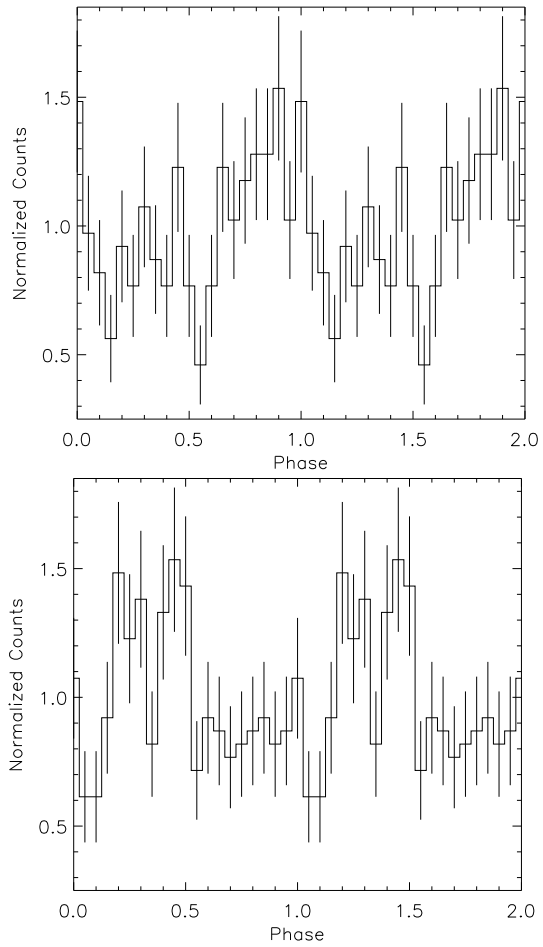


FIG. 8.— PN data in the 0.3–10 keV energy range for PSR B0355+54 folded on the frequency predicted from the radio measurements (top) and the frequency found from the $Z_1^2$-test (bottom). In both cases the data are folded using the radio ephemeris.

diffuse emission extending in the opposite direction to the pulsar's proper motion. Similar detections of extended emission have been seen for other sources (e.g. N157B, Wang & Gotthelf 1998; PSR B1757-24, Frail & Kulkarni 1991; Kaspi et al. 2001; PSR B1957+20, Stappers et al. 2003; PSR B1951+32, Li et al. 2005), and have been interpreted as emission from a ram-pressure confined PWN.

We cannot separate the core and diffuse emission components for the *XMM-Newton* data and find that the spectrum can be well-fitted with a power-law model with index $\Gamma = 1.5^{+0.5}_{-0.3}$, similar to the value found for other PWNe (Kaspi et al. 2005). The nebular emission is most likely dominating the spectrum. The core emission from the *Chandra* data can be well-fitted by a thermal plus power-law model. A fit with a blackbody plus power-law model gives $T = (2.32^{+1.16}_{-0.81}) \times 10^6$ K and $\Gamma = 1.0^{+0.2}_{-1.0}$. The fitted blackbody flux corresponds to an emitting radius of $0.12^{+0.16}_{-0.07}$ km, where the distance to the source is 1.04 kpc. In this case, the size of the emitting region implies that the flux originates from a hot polar cap. We can also fit the spectrum with a pure H, magnetized atmospheric plus power-law model. With the distance to the source fixed at 1.04 kpc, this fit results in $T^{\infty}_{eff} = (0.45^{+0.20}_{-0.22}) \times 10^6$ K, $\Gamma = 1.5^{+0.5}_{-0.4}$ and $R_{NS} = 7.2^{+7.2}_{-2.2}$ km. Taking into account the possible detection of pulsed emission from PSR B0355+54 it is likely that the emitting region is a hot polar cap.

It is suggested that the presence of a PWN is related to the spin-down power of the pulsar, and for sources with $\log \dot{E} \lesssim 36$ the PWN emission efficiency is significantly reduced (Frail & Scharringhausen 1997; Gaensler et al. 2000; Gotthelf 2003). For PSR B0355+54 $\log \dot{E} = 34.6$, making it one of a handful of sources with spin-down power below this limit with a detectable PWN (cf. Geminga, Caraveo et al. 2003). Using the results from the blackbody plus power-law fit to the core emission detected with *Chandra* we determine an isotropic unabsorbed luminosity in the 0.3–10 keV band of $8.3 \times 10^{30}$ erg s$^{-1}$. With $\dot{E} = 4.5 \times 10^{34}$ erg s$^{-1}$ for PSR B0355+54, this leads to a conversion efficiency of $2 \times 10^{-4}$. So in fact, we find that the conversion efficiency of the point source is similar to the values found for other pulsars (see e.g. Becker & Trümper 1997; Gaensler et al. 2004). Our analysis also indicates that the compact diffuse component is more luminous than the point source, with a conversion efficiency of $5 \times 10^{-4}$ in the 0.3–10 keV range. This result is again consistent with other sources (Becker & Trümper 1997). In addition, it is reported that when the pulsar spin-down energy is $\log \dot{E} \lesssim 36.5$ the morphology of the PWN seems to transition from toroidal to a jet/tail (Kaspi et al. 2005). Our measurements of PSR B0355+54 appear to agree with this trend.

The morphology of the diffuse emission depends on how the interaction with the interstellar medium (ISM) or supernova remnant constrains the flow of particles (e.g. Reynolds & Chevalier 1984). For a pulsar that is moving with a supersonic space velocity, the interaction of the supersonic flow with the ambient medium causes the speed of the flow to decrease sharply, while the density increases, forming a bow shock. In addition to the bow shock, which is at some distance ahead of the pulsar, a reverse shock is formed nearer to the source which terminates the pulsar wind.

The results of the spatial analysis of the *XMM-Newton* PN and *Chandra* ACIS data of PSR B0355+54 indicate that the bulk of the diffuse emission extends $\sim 50''$ [$0.25(d/1.04$ kpc) pc] downstream from the pulsar. Using the measurements of the pulsar's proper motion (Chatterjee et al. 2004) we find that the transverse velocity of PSR B0355+54 is $v_t = 61$ km s$^{-1}$. This implies that the time taken for the pulsar to have traversed the length of the diffuse emission is $> 4000$ yr. In addition, by considering the analysis of the *XMM-Newton* MOS1 data we find that the diffuse emission may extend as far as $\sim 5'$ [$1.51(d/1.04$ kpc) pc] from the point source. This results in a travel time of $> 24000$ yr for the pulsar. Following the work of Wang & Gotthelf (1998) (see also Kaspi et al. 2001) the synchrotron lifetime of an electron of energy $E$ (in keV) can be defined as $t_s \sim 40 E^{-1/2} B_{-4}^{-3/2}$ yr, where $B_{-4}^{-3/2}$ is the magnetic field in units of $10^{-4}$ G. Assuming that the dominant loss mechanism is synchrotron emission, i.e. $B > 3.2$ $\mu$G, and that the energy of the photon is $E \sim 5$ keV, then $t_s \sim 3000$ yr. This indicates that the diffuse emission that we detect is not due to particles deposited by the pulsar as it traveled through space. Hence, there

must be a constant supply of wind particles traveling at velocities greater than the space velocity of the pulsar. In addition, the particle flow velocity must be high enough such that the time for the flow to cross the length of the diffuse emission is less than the radiative lifetime of the particles.

Using the *Chandra* data we have modeled the spectrum of the compact diffuse emission, excluding the contribution from the pulsar, finding that the data can be well-fitted with a power-law. In other sources the power-law is seen to soften as one moves away from the pulsar position (see e.g. Slane et al. 2002; Li et al. 2005; Kaspi et al. 2005). An increase in the spectral index is expected as the particles will be cooler, i.e. older, at greater distance from the pulsar. Our results indicate that we are detecting relatively hard emission, but due to the uncertainties, we are unable to comment on any changes in the spectral slope. To measure cooling the PWN must be of an adequate size, it may be that for PSR B0355+54 the compact diffuse region is not large enough for a substantial change in power-law index to be measured, and there are too few counts in the more extended diffuse region to perform a spectral analysis. It is noted however that by comparing the spectral indices from the blackbody plus power-law fit to the core emission and the power-law fit to the compact diffuse emission we do detect an increase in $\Gamma$ of $\sim 0.5$.

Gaensler et al. (2004) have presented a detailed analysis of the diffuse X-ray emission associated with the radio source G359.23-0.82, also known as "the Mouse". Their hydrodynamic simulations show that there are a number of regions that can be defined in a pulsar bow shock. These include a pulsar wind cavity, shocked pulsar wind material, contact discontinuity (CD) and shocked ISM.

The energetic shocked particles from the pulsar are confined by the CD, the position of which denotes the transition to the shocked ISM. Following the method of Gaensler et al. (2004) we have estimated the distance between the peak of the emission from PSR B0355+54 and the sharp cut-off in brightness ahead of the pulsar. Using the same limit as Gaensler et al. (2004) i.e. where the X-ray surface brightness falls by $1/e^2 = 0.14$, we find a distance of $0.9'' \pm 0.2''$, giving the CD a projected radius of $r_{\rm CD} = 0.004 \pm 0.001$ pc. Here, and in the following, we have used a distance to the pulsar of 1.04 kpc (Chatterjee et al. 2004). From Eq. (1) of Gaensler et al. (2004) we can estimate the radius of the forward termination shock (TS), $r^F_{\rm TS} \sim 0.003$ pc. This corresponds to an angular distance of $\theta = 0.59''$. Comparing our values to those for the Mouse implies that the emission in front of the pulsar is more compact in PSR B0355+54 than for the Mouse. In both cases the close proximity of the forward TS to the peak X-ray emission renders the TS undetectable. Using our results and Eq. (2) of Gaensler et al. (2004) we find that PSR B0355+54 produces a ram pressure of $\rho v_t^2 \sim 1.4 \times 10^{-9}$ ergs cm$^{-3}$. Assuming cosmic abundances, this gives $v_t \sim 247 n_0^{-1/2}$ km s$^{-1}$, where $n_0$ is the number density of the ambient medium, so for PSR B0355+54 we determine $n_0 \approx 0.06$ cm$^{-3}$, which is not unrealistic.

Additional information can be obtained by equating the pressure of the pulsar wind (assumed isotropic), to that of the ambient medium. By introducing the Mach number $M = v_t/c_s$, where $c_s$ is the adiabatic sound speed in the ambient medium, and using the same prescription as Gaensler et al. (2004) for a representative ISM pressure (i.e. $P_{ISM} = 2400 k P_0$ erg cm$^{-3}$, with $0.5 \lesssim P_0 \lesssim 5$ and $k$ is the Boltzmann's constant), this gives:

$$\dot{E}/[4\pi (r^F_{TS})^2 c] = 2400 k \gamma_{ISM} P_0 M^2 \,, \qquad (1)$$

from which we can obtain an estimate of the Mach number. We find that for PSR B0355+54 the sound speed $c_s$ of the medium lies in the range $1 - 30$ km s$^{-1}$. The three principal phases of the ISM are generally named cold, warm and hot and are characterized by typical sound speed values of 1, 10 or 100 km s$^{-1}$; according to this denomination our result implies that the pulsar is moving in either a cold or mildly warm ambient gas. For comparison, in the case of the Mouse, Gaensler et al. (2004) found that the most probable pulsar velocity requires that the pulsar is moving through a warm phase of the ISM.

Gaensler et al. (2004) also discuss the possible detection of the backward TS in their data. Their simulations show that this feature has a closed surface, while the CD and bow shock are unrestricted. The backward TS should lie much further away from the pulsar than the forward TS, i.e. $r^B_{\rm TS} \gg r^F_{\rm TS}$. In principle this means that the backward TS may be detectable. The possible dip we see in the profiles for the PSR B0355+54 data could indicate the presence of the backward TS. The angular separation of the dip in our data is $\sim 10''$, a value consistent with that for the Mouse. For a backward TS, Gaensler et al. (2004) predict that there would be a lack of spectral evolution, a result we have found for the diffuse emission of PSR B0355+54. However, we note that the feature in the Mouse data (and simulations) is quite compact in the north-south direction in comparison to the PSR B0355+54 feature. In addition, the number of counts we detect for PSR B0355+54 may hinder our investigation of the presence of such a feature. Deeper observations are needed to probe further the PWN of PSR B0355+54.

A few days before submission of this paper, Tepedelenlioğlu & Ögelman submitted a paper based on the same (public) observations to ApJL (astro-ph/0512209).

The authors wish to thank the referee for useful comments that have helped improve the paper. This work is based on observations obtained with *XMM-Newton*, an ESA science mission with instruments and contributions directly funded by ESA Member States and NASA. Support for this work was provided by the National Aeronautics and Space Administration through Chandra Award Number NNG04EF62I issued by the Chandra X-ray Observatory Center, which is operated by the Smithsonian Astrophysical Observatory for and on behalf of the National Aeronautics Space Administration under contract NAS8-03060. SZ thanks PPARC for its support through a PPARC Advanced Fellowship

REFERENCES

Becker, W., Trümper, J. 1997, A&A, 326, 682

Bhat, P. N., Acharya, B. S., Gandhi, V. N., Ramana Murthy, P. V., Sathyanarayana, G. P., Vishwanath, P. R. 1990, A&A, 236, 1

Buccheri, R., et al. 1983, A&A, 128, 245
Caraveo, P. A., Bignami, G. F., DeLuca, A., Mereghetti, S., Pellizzoni, A., Mignani, R., Tur, A., Becker, W. 2003, Science, 301, 1345
Cash, W. 1979, ApJ, 228, 939
Chatterjee, S., Cordes, J. M., Vlemmings, W. H. T., Arzoumanian, Z., Goss, W. M., Lazio, T. J. W. 2004, ApJ, 604, 339
de Jager, O. C. 1991, ApJ, 378, 286
Frail, D. A., Kulkarni, S. R. 1991, Nature, 352, 785
Frail, D. A., Scharringhausen, B. R. 1997, ApJ, 480, 364
Gaensler, B. M., Stappers, B. W., Frail, D. A., Moffett, D. A., Johnston, S., Chatterjee, S. 2000, MNRAS, 318, 58
Gaensler, B. M. 2001, in Young Supernova Remnants, eds. S. S. Holt & U. Hwang, AIP Conference Proceedings, 565, 295
Gaensler, B. M., van der Swaluw, E., Camilo, F., Kaspi, V. M., Baganoff, F. K., Yusef-Zadeh, F., Manchester, R. N. 2004, ApJ, 616, 383
Gotthelf, E. V. 2003, ApJ, 591, 361
Helfand, D. J. 1983, in IAU Symp. 101, Supernova Remnants and Their X-ray Emission, eds. J. Danzinger & P. Gorenstein, Dordrecht: Reidel, 471
Hobbs, G., Lyne, A. G., Kramer, M., Martin, C. E., Jordan, C. 2004, MNRAS, 353, 1311
Kaspi, V. M., Gotthelf, E. V., Gaensler, B. M., Lyutikov, M. 2001, ApJ, 562, 163
Kaspi, V. M., Roberts, M. S. E., Harding, A. K. 2005, in Compact Stellar X-ray Sources, ed. W. H. G. Lewin & M. van der Klis (Cambridge: Cambridge Univ. Press), in press
Li, X. H., Lu, F. J., Li, T. P. 2005, ApJ, 628, 931
Manchester, R. N., Hobbs, G. B., Teoh, A., Hobbs, M. 2005, AJ, 129, 1993
Mardia, K. V. 1972, Statistics of Directional Data (London: Academic)
Pavlov, G. G., Shibanov, Y. A., Zavlin, V. E., Meyer, R. D. 1995, in The Lives of Neutron Stars eds. A. Alpar, U. Kilizóglu & J. van Paradijs, Kluwer Academic Publishers, p. 71
Pavlov, G. G., Kargaltsev, O. Y., Sanwal, D., Garmire, G. P. 2001, ApJ, 554, 189
Rees, M. J., Gunn, J. E. 1974, MNRAS, 167, 1
Reynolds, S. P., Chevalier, R. A., 1984, ApJ, 278, 630
Seward, F. D., Wang, Z.-R. 1988, ApJ, 332, 199
Slane, P. 1994, ApJ, 437, 458
Slane, P. O., Helfand, D. J., Murray, S. S. 2002, ApJ, 571, 45
Stappers, B. W., Gaensler, B. M., Kaspi, V. M., van der Klis, M., Lewin, W. H. G. 2003, Sci, 299, 1372
Strüder, L., et al. 2001, A&A, 365, L18
Tepedelenlioğlu, E., Ögelman, H. 2005, ApJL, submitted (astro-ph/0512209)
Turner, M. J. L., et al. 2001, A&A, 365, 27
Wang, Q. D., Gotthelf, E. V. 1998, ApJ, 494, 623
Weisskopf, M. C. 2000, ApJ, 536, 81
Zane, S., et al. 2002, MNRAS, 334, 345